Pressure effects on kinetics and decay processes in krypton after selective photoexcitation

E. Audouard, P. Laporte, J.L. Subtil, and N. Damany

Citation: The Journal of Chemical Physics **89**, 6176 (1988); doi: 10.1063/1.455434
View online: http://dx.doi.org/10.1063/1.455434
View Table of Contents: http://scitation.aip.org/content/aip/journal/jcp/89/10?ver=pdfcov
Published by the AIP Publishing

Pressure effects on kinetics and decay processes in krypton after selective photoexcitation

E. Audouard, P. Laporte, J.-L. Subtil, and N. Damany
Equipe de Spectroscopie, C. N. R. S. (U. A. 171), Universités de Saint-Etienne et de Lyon I, 158 bis Cours Fauriel, 42023 Saint-Etienne Cédex, France

(Received 23 May 1988; accepted 15 July 1988)

Kinetics associated with the decay of the $5s[3/2]_1^0$ ($^3P_1$) excited state of krypton is investigated using selective excitation, in the density range 2.5×10^{18} to 375×10^{18} atoms cm^{-3} (pressure from 10^4 to 1.5×10^6 Pa). The vacuum ultraviolet (VUV) one-photon excitation around 123.6 nm is provided by monochromatized light from a laser-generated rare gas plasma. The basic experimental data are obtained through the time-resolved second continuum excimer fluorescence at 145 nm. When initial conditions give purely $^3P_1$ atomic excitation a single slow component is observed at densities up to 15×10^{18} cm^{-3}, corresponding to the $1_u,0_u^-$, $v=0$ excimer radiative decay (265 ns). From 15 to 60×10^{18} cm^{-3}, a second fast component shows up, corresponding to the 0_u^+ ($^3P_1$), $v=0$ excimer radiative decay. Above 60×10^{18} cm^{-3} the intensity ratio between the two components remains constant (F/S$\approx$0.21). Behavior rather similar to that previously reported for argon and xenon is found. In particular one concludes that the $^3P_2$ atomic state plays a major role as an intermediate state in the $1_u,0_u^-$ dimer formation whereas possible short-distance attractive g states do not seem to play any significant role. A self-consistent analysis leads to a detailed quantitative description of the kinetics. In particular, it is found that dimer formation times from $^3P_1$ and $^3P_2$ atomic states are in the ratio 3/1. In the considered density range collisional rates are found to vary quadratically.

I. INTRODUCTION

In spite of current interest in rare gases excited state kinetics, studies on krypton are relatively scarce and the very basic processes still remain poorly known. The present paper is the third of a series. The two preceding works were devoted to argon[1] and xenon,[2] and were performed by selective photoexcitation in a large range of density. That was found to be essential to reach unicity of the decay scheme, and, subsequently, to give a reliable interpretation of the characteristic times involved. Actually, this is a crucial question since various models relying mainly on nonselective experiments have been proposed. An extensive bibliography on the subject is contained in Refs. 1 and 2.

For the $^3P_1$ atomic state decay, the same scheme was found for argon and xenon, whereas a very different behavior was observed for their $^1P_1$ states decays, i.e., the evidence for a rather long-lived $^3P_0$ reservoir in argon, which is not observed in xenon due to the closely lying $6p$ level manifold.

As expected, the same general features as for argon and xenon are observed for the data associated with the selective excitation of the $3P_1$ state of krypton. The $^1P_1$ state excitation clearly reveals, like for argon, a long-lived reservoir for which additional experiments, modeling, and previous $^3P_1$/$^3P_2$ kinetics knowledge are needed. Further work is still under way so that only preliminary results will be given about $^1P_1$ decay in the present paper. Even at this stage the reservoir effect associated with the $^1P_1$ decay strengthens the need of a selective $^3P_1$ excitation study and underlines a major difficulty when interpreting nonselective excitation experiments: Actually, in such studies the excitation conditions are not well defined and most of initial excitation is contained in highly excited and ionic species.

The kinetic scheme associated with the $^3P_1$ level decay of argon[1] and xenon[2] may be expected to hold again for krypton due to close basic similarity. For the sake of clarity, we adopt in this paper a presentation somewhat different from that adopted in Refs. 1 and 2: After describing the experiment we shall recall the decay scheme used in these works since it will be demonstrated that it also holds in the case of krypton. Doing so will allow us then to underline more clearly the improvements brought about the mathematical model.

II. EXPERIMENTAL

A. Principle of the experiment

One-photon VUV excitation of the lowest-lying atomic excited states of krypton and/or of the correlated molecular states is performed in the neighborhood of the first two levels, $^3P_1$, $^1P_1$, for which resonant transitions from the ground state occur, according to the energy level diagram sketched in Fig. 1. The potential energy curves are taken from Ref. 3. According to the quasistatic theory, excitation on the high energy side (blue wing excitation) of both resonant transitions gives rise to dissociative pairs so that, in practice, a purely atomic initial excitation can be considered. Conversely, a red wing excitation leads to the Kr_2^* (0_u^+, $v\gg0$) bound excimer formation in high vibrational levels. Initial conditions are then not well defined since quite a large number of vibrational levels are populated with the instrumental width of 0.7 nm. Nevertheless, such an information remains very helpful as will be seen later. In addition, in case of excitation since the transition moment is no more negligible at intermediate distance.[3]

After excitation the decay takes place via various pro-

 0021-9606/88/226176-13$02.10

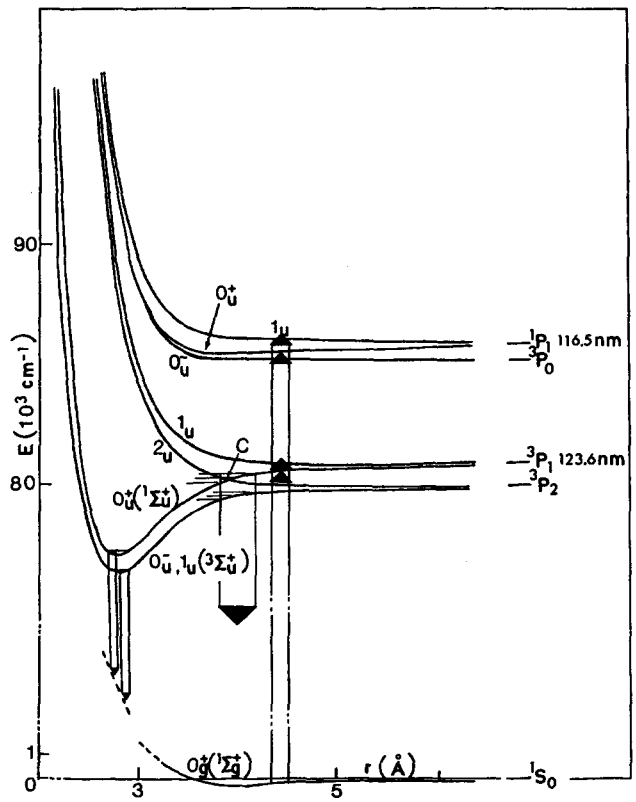

FIG. 1. Atomic energy levels, molecular potential energy curves, and transitions involved in the present experiments.

cesses: radiation trapping, excimer formation and relaxation, excimer dissociation, and VUV fluorescence. At very low pressure, not considered here, emission from the relaxed 0_u^+ ($^1P_1$) excimer may take place in the case of $^1P_1$ excitation.[4] The first continuum emission, arising from 0_u^+, $v \gg 0$ ($^3P_1$) radiative decay around $\lambda = 125$ nm (Fig. 1) also occurs at low and intermediate density ($d < 50 \times 10^{18}$ cm^{-3}).

Depending on density, part of or all the excitation is finally transferred to the two relaxed excimer states 0_u^+ and $1_u, 0_u^-$ ($v = 0$), the radiative decay of which gives the two temporal components of the so-called second continuum (Fig. 1). The present study is fully based on the experimental observation of the time-resolved second continuum when varying the excitation wavelength and the density.

B. Experimental setup

As stated above the use of selective excitation is a major point in this study. The improved spark source used in our previous work on argon[1] is not fast enough to provide sufficient contrast between the two components of the krypton excimer second continuum. Laser excitation was not retained for the following reasons:

(i) rather short wavelengths required for two-photon $5p$ krypton atomic excitation;

(ii) $^3P_1$ and $^1P_1$ states do not act as final states in case of three-photon excitation but mainly as intermediate states for higher order processes (see, for instance, Ref. 5). Then the selective character of the excitation is lost.

The rare gas plasma laser VUV source we recently described[6] was conveniently used with the only drawback of a still rather large time width, typically 20 and 30 ns with neon and argon, respectively. Indeed, its very good pulse to pulse reproducibility allows an accurate account of the pulse shape into the convolution routine.

Briefly, the plasma is generated by focusing, with a 35 mm focal length lens, ~300 mJ of a 20 Hz Nd–YAG laser beam (YG 581 from Quantel) into a cell containing either neon or argon at pressures 500 or 100 kPa, respectively.

The experimental setup (Fig. 2) is similar to that described in Ref. 1, except that the entrance slit of the monochromator is removed. Indeed, as the laser beam propagates vertically in the source chamber, the plasma may roughly be assimilated to a cylinder of typical width 0.7 mm and height 7 mm, in place of the entrance slit. A bandpass of 0.7 nm is selected by a 1 m VUV monochromator equipped with a 1 mm width exit slit.

The cross-shaped fluorescence cell is high-vacuum, high-pressure compatible and is operated at room temperature. Its entrance window (MgF_2, optical cutoff at $\lambda \sim 115$ nm) is put just beyond the exit slit of the monochromator. The dispersed fluorescence is observed at right angle through a BaF_2 filter; its cutoff at 135 nm prevents detection of all parasitic light possibly scattered from the excitation beam or emitted in the first continuum (~125 nm). The fluorescence emission in the second continuum, centered near 145 nm, is detected either by a photomultiplier equipped with a CsI photocathode or by microchannel plates also equipped with an additional photocathode.[7] The spectral sensitivity is then limited to the 135–190 nm range, suitable for detecting the fluorescence of the second continuum only. Ultrapure krypton (N50 grade) containing less than 5 ppm of xenon was supplied by Air Liquide (France), and used without further purification.

The fluorescence is time analyzed with a Tektronix 7912 AD fast transient digitizer coupled to a microcomputer. The entire temporal spectrum being recorded for each laser shot, all errors due to source fluctuations are removed, and good statistics are generally obtained after typically 1000 pulses.

The source instrumental response function, used for the convolution procedure, is recorded at the excitation wavelength by removing the BaF_2 filter, and introducing at the cell entrance a scattering element—e.g., a thin metallic wire—adapted in such a way that counting a rate compara-

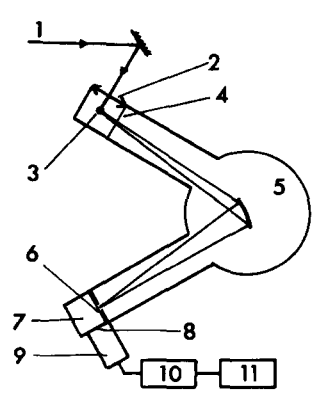

FIG. 2. Experimental setup. (1) light beam from the Quantel Nd–YAG laser; (2) focusing lens; (3) neon or argon plasma (actually the laser beam propagates parallel to grating grooves, so that the plasma acts as an entrance slit for the monochromator); (4) MgF_2 window; (5) monochromator; (6) MgF_2 window; (7) krypton cell; (8) BaF_2 filter; (9) fluorescence detector (PM or MCP); (10) fast transient digitizer; (11) computer and plotter.

ble to that of the experiment. So, it contains the contribution of both the excitation source and the whole detection system.

Figure 3 shows examples of fluorescence curves obtained at very different densities in the case of blue wing excitation. At low density only one component is observed [Fig. 3(I)] whereas at high density the curve exhibits both fast and slow components [Fig. 3(II)].

III. KINETIC DIAGRAM

A. Basic processes

The model we have retained rests on *ab initio* potential energy curves calculated by Gadea *et al.*[3] in which the g states have no significant well and lie entirely above their dissociation limits. The analysis of our experimental data will allow to conclude that there is actually no short-distance g state contribution to kinetics.

The decay sequence associated with the $^3P_1$ atomic state excitation takes place according to the basic scheme, sketched in Fig. 4, originally introduced by Wenck *et al.* (xenon),[8] by Haaks (xenon and krypton),[9] and extended recently to argon.[1] The processes involved in the decay sequence are reviewed, introducing the K_i rates associated with the processes (p_i). The first step (p_1) is the dimer formation, in a high vibrational level, from free atoms. It is

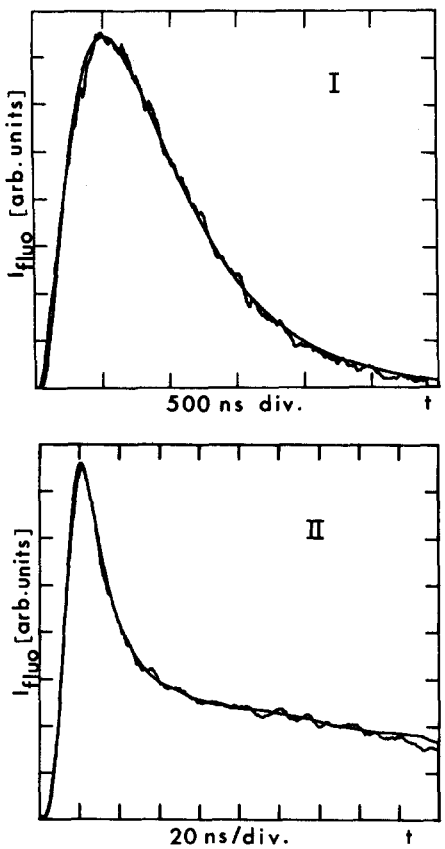

FIG. 3. Time-resolved fluorescence signal (second continuum) after excitation at $\lambda = 122.6$ nm, with the curve resulting from the fitting procedure superimposed on the experimental one. (I) $d = 9\times10^{18}$ cm^{-3}. Fast component: absent. Slow component: $\tau_r = 350$ ns, $\tau_d = 370$ ns. (II) $d = 200\times10^{18}$ cm^{-3}. Fast component: $\tau_r = 1.1$ ns, $\tau_d = 3.6$ ns. Slow component: $\tau_r = 1.4$ ns, $\tau_d = 265$ ns.

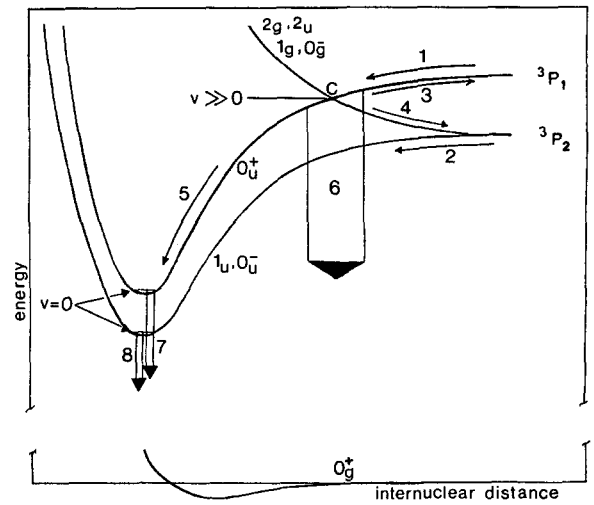

FIG. 4. Kinetic diagram associated with the $^3P_1$ atomic excitation. For explanation of the various processes, see the text.

expected to take place through three-body collisions as confirmed by the analysis:

$$Kr^*(^3P_1) + 2Kr(^1S_0) \xrightarrow{K_1} Kr_2^*(0_u^+, v \gg 0) + Kr(^1S_0)\,. \qquad (p_1)$$

Then there is competition between the four following processes:

(i) Collision induced dissociation to $^3P_1$:

$$Kr_2^*(0_u^+, v \gg 0) + Kr(^1S_0) \xrightarrow{K_3} Kr^*(^3P_1) + 2Kr(^1S_0)\,; \qquad (p_3)$$

(ii) collision induced dissociation to $^3P_2$:

$$Kr_2^*(0_u^+, v \gg 0) + Kr(^1S_0) \xrightarrow{K_4} Kr^*(^3P_2) + 2Kr(^1S_0)\,; \qquad (p_4)$$

(iii) collision induced vibrational relaxation to $v = 0$:

$$Kr_2^*(0_u^+, v \gg 0) + Kr(^1S_0) \xrightarrow{K_5} Kr_2^*(0_u^+, v = 0) + Kr(^1S_0)\,; \qquad (p_5)$$

(iv) direct radiative decay (first continuum):

$$Kr_2^*(0_u^+, v \gg 0) \xrightarrow{K_6} 2Kr(^1S_0) + h\nu\,. \qquad (p_6)$$

The process (p_4) was proved to be very efficient for argon and xenon. It relies on the possibility of collision induced symmetry change leading to dissociation through one of the four $1_g, 0_g^-, 2_g, 2_u$ molecular states, correlated to the $^3P_2$ level, which are expected to be purely repulsive, at least for the distances considered.[3,10,11] This effect is schematically represented as taking place in the neighborhood of the crossing point C (Fig. 4).

The relaxed excimer issued from process (p_5) radiates:

$$Kr_2^*(0_u^+, v = 0) \xrightarrow{K_{0_u^+}} 2Kr(^1S_0) + h\nu\,. \qquad (p_7)$$

As for the $Kr^*(^3P_2)$ excited atoms, they decay through

sequence analogous to the $(p_1)(p_5)(p_7)$ one, that we shall reduce to a two-step process:

(1) Dimer formation and relaxation:

$$Kr^*(^3P_2) + 2Kr(^1S_0) \xrightarrow{K_2}$$

$$Kr_2^*(1_u 0_u^-, v=0) + Kr(^1S_0)\,; \qquad (p_2)$$

(2) relaxed excimer radiative decay:

$$Kr_2^*(1_u, 0_u^-, v=0) \xrightarrow{K_{1u}} 2Kr(^1S_0) + h\nu\,. \qquad (p_8)$$

Indeed the one-step process (p_2) equivalent to $(p_1) + (p_5)$ can be introduced since, as it will be checked later:

(1) radiative decay from 1_u, $v \gg 0$ levels is negligible in the density range of our observation (no loss process);

(2) all the collisional processes invoked will be found to be quasiquadratic vs pressure, so that a single decay constant may be introduced for the $^3P_2$ collisional decay to the relaxed 1_u excimer (p_2).

Finally, this scheme neglects (1) binary collision induced decay from $^3P_1$ to $^3P_2$; (2) collisional mixing between 0_u^+ and $1_u, 0_u^-$ excimer states at intermediate $(v \gg 0)$ or short $(v=0)$ internuclear distances; and (3) g-type bound excimers at short distance as previously mentioned.

These statements will now be discussed.

B. Preliminary conclusions deduced from raw data

From the observation of the fluorescence curves obtained in the case of red wing excitation it is possible to deduce preliminary information without the help of a mathematical model. If an efficient physical process takes place at the neighborhood of point C, clear change in the respective contributions of the fast and the slow components must occur when exciting on either side of C. In spite of limited spectral resolution such an effect is clearly observed. Figure 5 corresponds to data obtained at rather high density. It clearly exhibits a large effect on the respective contribution of the fast and slow components at a density where the kinetic decay times are sufficiently small so that they no longer play a role in the temporal shapes which are instrumental width limited. Only the hypothesis of dissociation in the neighborhood of point C is compatible with such a behavior. Direct evidence of that dissociation process has been recently reported for xenon[2] using two-step excitation techniques. Figure 6 is deduced from the data illustrated in Fig. 5 from the variation of integrated intensity associated with peak-intensity normalized curves. The steep drop of the curve in Fig. 6 occurs at excitation wavelength larger than $\lambda_0 = 123.58$ nm ($^3P_1$ atomic state excitation wavelength). We may estimate that the edge at nearly 124 nm corresponds to the red tail of an excitation band centered at λ_c. Assuming roughly a triangular spectral distribution would lead to estimate λ_c at $124 + 0.7$ nm ($E_c = 80\,190\ \mathrm{cm}^{-1}$) which is consistent with what can be expected from *ab initio* calculation.[3,10,11] For excitation wavelength ranging from λ_0 to λ_c, at a fixed density low enough to involve rather long kinetic times, the rise time of the fluorescence signal decreases when the excitation wavelength increases as illustrated by curves (a) and (b) in Fig. 7. This behavior can only be explained by a shortening of the time associated with process (p_1), resulting from direct high-v, bound-excimer formation. At low density that effect involves time variations which may reach hundreds of nanoseconds. This means that (p_1) involves rather long times as compared to other kinetic times, results which will be quantitatively established from the analysis of blue wing excitation data. As for curve (c) in Fig. 7, it corresponds to excitation at $\lambda > \lambda_c$ where the residual slow component contribution arises only from direct 1_u, $v \gg 0$ excitation, since the corresponding absorption coefficient is not negligible.[3] The very short kinetic times involved are consistent with the diagram of Fig. 4.

It is important to notice that the behavior of time-resolved fluorescence resulting from red wing excitation just discussed would not be observed if any of the neglected processes mentioned at the end of Sec. III A was efficient. Indeed, a binary collision induced decay from $^3P_1$ to $^3P_2$ would cancel the slow component as soon as an excitation wave-

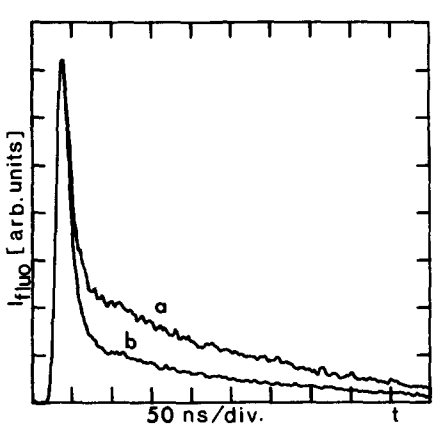

FIG. 5. Time-resolved fluorescence resulting from $^3P_1$ red wing excitation ($d = 200\times10^{18}\ \mathrm{cm}^{-3}$). (a) $\lambda_{exc} = 124.1$ nm; (b) $\lambda_{exc} = 125.6$ nm.

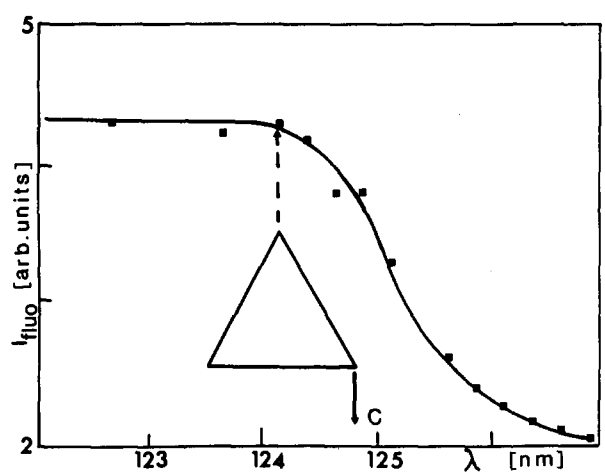

FIG. 6. Time-integrated fluorescence intensity vs excitation wavelength when normalizing fast component peak intensities. For C point positioning, the spectral distribution of the excitation is approximated by the drawn triangular function (FWHM = 0.7 nm).

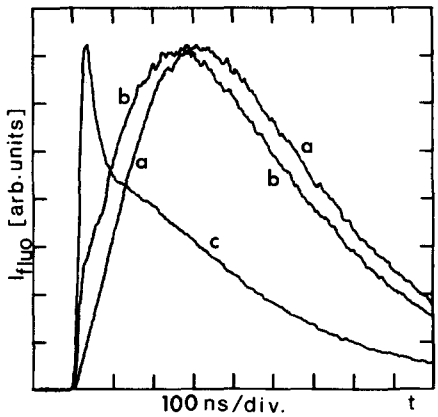

FIG. 7. Time-resolved fluorescence resulting from red wing excitation ($d = 15\times10^{18}$ cm^{-3}). (a) $\lambda_{exc} = 123.1$ nm; (b) $\lambda_{exc} = 124.1$ nm; (c) $\lambda_{exc} = 125.6$ nm.

length $\lambda > \lambda_0$ is considered, and the same holds for g state well effects. As for collisional mixing between 0_u^+ and $1_u, 0_u^-$ states at short and intermediate distances, it would lead to, respectively, either a constant ratio of the two components or a steadily varying effect when exciting at a wavelength increasingly larger than λ_0. The discussion concerning blue wing excitation data will confirm these preliminary conclusions.

IV. KINETIC MODELING

We have now to settle mathematical expressions which both accomodate the adopted kinetic diagram and allow the decay scheme to fit experimental fluorescence curves.

Indeed, any decay is known to be a combination of exponential terms and we should, in principle, analyze the corresponding curves with impulse responses being a combination of as many exponential terms as there are states involved in the decay sequence. Actually such a treatment is clearly unrealistic for a sequence involving a great number of rovibronic levels. So we have to describe, in a simplified way, all the basic processes involved. In practice, it has been repeatedly stated in numerous works that no more than three exponential terms could be deduced unequivocally from a one-component fluorescence curve while it is obvious that at least two exponential terms are necessary.

We shall introduce two mathematical expressions adapted to the description of the various regimes which can be distinguished in the experiment depending on the presence of one or two components in the fluorescence.

A. Slow component description by a three-exponential model

According to Fig. 4, the decay scheme of the slow component may be sketched as indicated in Fig. 8(I). Here K is introduced to represent the loss rates relative either to the first continuum emission K_6 or to the relaxation rate K_5 increasingly effective when going from low to high density.

Let $v_0(t)$, $v_1(t)$, $v_2(t)$, and $v_3(t)$ be the population at time t of, respectively, $1_u, 0_u^-$ $v = 0$, $^3P_2$, 0_u^+ $v \gg 0$, $^3P_1$ states involved in the scheme of Fig. 8(I). The emission $v_0(t)$ of the

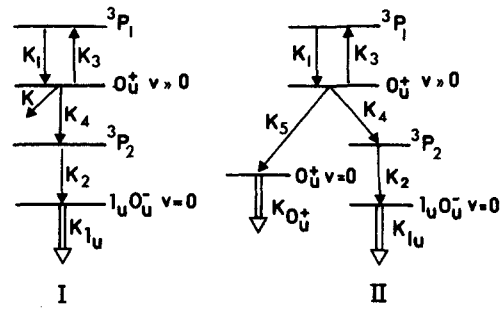

FIG. 8. Schematic representation of the decay sequence. (I) slow component decay sequence. (II) Coupling of slow and fast component decay sequences.

lower level is obtained by solving the following matrix equation:

$$\frac{d}{dt}\begin{pmatrix} v_3(t) \\ v_2(t) \\ v_1(t) \\ v_0(t) \end{pmatrix} = M \begin{pmatrix} v_3(t) \\ v_2(t) \\ v_1(t) \\ v_0(t) \end{pmatrix}, \tag{1}$$

where

$$M = \begin{pmatrix} -K_1 & K_3 & 0 & 0 \\ K_1 & -K_s & 0 & 0 \\ 0 & K_4 & -K_2 & 0 \\ 0 & 0 & K_2 & -K_{1_u} \end{pmatrix},$$

$$K_s = K + K_3 + K_4,$$

and

$$\begin{pmatrix} v_3(0) \\ v_2(0) \\ v_1(0) \\ v_0(0) \end{pmatrix} = \begin{pmatrix} N_0 \\ 0 \\ 0 \\ 0 \end{pmatrix},$$

N_0 being the initial number of excited species.

The v_0 function is expressed as the sum of four exponential terms whose arguments are the eigenvalues of the matrix M, i.e.,

$$\{-(K_s + K_1) \pm [(K_s + K_1)^2 - 4K_1(K_s - K_3)]^{1/2}\}/2, -K_2, -K_{1_u}.$$

The first step is to reduce the number of exponentials from four to three, which is possible by comparing K_s to K_1, K_2, and K_{1_u}.

If $K = K_6$ (low density), $K_s = K_3 + K_4 + K_6$. From the works of Bonifield *et al.*,[12] Matthias *et al.*,[13] and Gadéa *et al.*,[3] one may estimate that $K_6^{-1} = \tau_6 = 3.3$ ns. In the corresponding density range, collisional processes cannot lead to such a short time, which is also shorter than the (relaxed) 1_u state radiative lifetime τ_{1_u} (> 100 ns). So one has

$$K_s > K_6 \gg K_1, K_2, \text{ and } K_{1_u}.$$

When the density increases, the rates K_1 and K_2 can

become higher than K_6, owing to collisional processes, but, simultaneously, $K \approx K_5$. Furthermore, process (p_4) is obviously an efficient process since it monitors the slow component, and one may expect that (p_4) and (p_5) processes are faster than dimer formation (p_1), (p_2), which will be fully confirmed by the analysis. So one may write at high density,

$$K_s > K_5 + K_4 \gg K_1, K_2, \text{ and } K_{1u}.$$

Finally, in the whole density range, $K_1 \ll K_s$. This condition allows easier $v_0(t)$ calculation leading to

$$v_0(t) = A[I_{K+} \exp(-K_+ t) + I_{K2} \exp(-K_2 t) + I_{K1u} \exp(-K_{1u} t) + I_{K-} \exp(-K_- t)] \quad (2)$$

with

$$K_+ = \{(K_s + K_1) - [(K_s + K_1)^2 - 4K_1(K_s - K_3)]^{1/2}\}/2 \approx \alpha K_1, \quad \alpha = (K_4 + K)/K_s$$

and

$$K_- = \{(K_s + K_1) + [(K_s + K_1)^2 - 4K_1(K_s - K_3)]^{1/2}\}/2 \approx K_s.$$

The I_K may be expressed as

$$I_{K+} = [(K_2 - K_+)(K_{1u} - K_+)]^{-1},$$
$$I_{K2} = -[(K_2 - K_+)(K_{1u} - K_2)]^{-1},$$
$$I_{1u} = [(K_{1u} - K_2)(K_{1u} - K_+)]^{-1},$$
$$I_{K-} = [(K_s - K_2)(K_s - K_{1u})]^{-1},$$

and the coefficient A:

$$A = K_1 K_2 K_4 N_0 / K_s = K_2 N_0 [K_4/(K_4 + K)][(K_4 + K)/K_s] K_1.$$

With $N_0' = N_0 K_4/(K_4 + K)$, one gets

$$A = K_2 N_0' (K_4 + K) K_1 / K_s = K_2 N_0' \alpha K_1.$$

Two cases have to be considered:

(i) $K = K_6$ (low density), then $K \gg K_4$ is possible so that $N_0' \ll N_0$ can occur. It illustrates the loss of excited species via the first continuum and the vanishing of the slow component at very low density.

(ii) $K = K_5$ (high density), then $N_0 - N_0'$ represents the excited species which feed the fast component.

Now let us examine the coefficient α in the same manner and define the values corresponding to low and high densities, respectively,

$$\alpha_L = (K_4 + K_6)/(K_3 + K_4 + K_6),$$
$$\alpha_H = (K_4 + K_5)/(K_3 + K_4 + K_5).$$

K_6 is the highest rate in the range where it has to be considered so that $\alpha_L \approx 1$.

As for the other case, we recall that K_3 corresponds to the dissociation process (p_3), from the point C (Fig. 4) to $^3P_1$. Either *ab initio* calculations or estimation deduced from Fig. 6 indicates consistently that the energy difference between C and $^3P_1$ is several hundreds of cm^{-1} so that the process cannot be very efficient as compared to processes (p_4) and (p_5), therefore, $K_4 + K_5 \gg K_3$ and then $\alpha_H \approx 1$. So, *in the whole density range, one has* $K_+ \approx K_1$ Since $K_- \approx K_s \gg k_+ \approx K_1$, $K_- \gg K_2$, and $K_- \gg K_{1u}$, one has

$$I_{K-} \approx K_s^{-2} \ll I_{K1}, I_{K2}, I_{K1u}$$

and

$$\exp(-K_- t) \ll \exp(-K_i t) \quad (i = 1, 2, 1_u).$$

So we can write

$$v_0(t) \approx I_1(t) = K_2 K_1 N_0' [(K_2 - K_1)^{-1} \times (K_{1u} - K_1)^{-1} \exp(-K_1 t) - (K_2 - K_1)^{-1}(K_{1u} - K_2)^{-1} \exp(-K_2 t) + (K_{1u} - K_2)^{-1}(K_{1u} - K_1)^{-1} \exp(-K_{1u} t)]. \quad (3)$$

I_1 is the impulse response to $^3P_1$ excitation through the three-level system ($^3P_1$, $^3P_2$, $1_u v = 0$).

So we may expect that, at rather low density, the first continuum emission (p_6) is so efficient that the fast component of the relaxed excimer emission (p_7) is totally cancelled, and then, the observed second continuum emission contains the slow component only.

It is important to notice that, in this formula, the K_i are already affected to specific physical processes of the kinetic diagram. Furthermore, the coefficients in front of the exponentials are not free in contrast with that of the formula widely used in previously published studies on kinetics, i.e.,

$$I(t) = \sum_{j=1,3} I_j \exp(-K_j t), \quad (4)$$

where five parameters have to be fitted.

Using formula (3) we got good fits at low density up to 15×10^{18} cm^{-3}. The impossibility to get a good fit at higher density was ascribed to the rise of the fast component. Nevertheless, this model is expected to hold for the description of the slow component even at high density.

B. Two-component description by a (2×2)-exponential model

For densities above 15×10^{18} cm^{-3} (60 kPa) a two-component fluorescence signal like that given in Fig. 3 (II) has to be fitted. According to the scheme of Fig. 4 the decay sequence can be sketched as reported in Fig. 8(II), with the coupling of two deexcitation channels. The relative efficiency of the radiative process (p_6) decreases rapidly since K_6 is not density dependent, and it vanishes totally above 60×10^{18} cm^{-3}. In practice, the fitting procedure reveals that in the density range $(15–50) \times 10^{18}$ cm^{-3} poor accuracy is obtained due to the overlapping of both the slow and the fast components. Therefore, the fitting procedure will be useful, mainly above 50×10^{18} cm^{-3}, when the process (p_6) does not have to be taken into account.

According to the kinetic diagram, the fast component corresponds to a three-level system ($^3P_1$, 0_u^+ $v \gg 0$, 0_u^+ $v = 0$) and has to be described by three exponentials. Describing again the slow component with three exponentials a total of six exponentials would be used now. Actually, owing to the imbrication of the components, we should have trouble with unicity and interpretation. Unhappily, it is no longer possible to reduce the number of exponentials by the procedure presented above since no further simplifying

assumption holds in the whole density range. So, we again use the procedure introduced in Ref. 2 which reduces the number of exponentials with, as a counter part, the need for interpreting the fitted rate parameters.

In this method (see the Appendix in Ref. 2), $I_1(t)$, being the exact solution of the three-level system $g(t) = \alpha \exp(-Kt) + \beta \exp(-K't)$, is defined by a minimization system:

$$m(K,K') = \int_0^\infty [I_1(t) - g(t)]^2 \, dt,$$

$$\delta m/\delta K = 0, \quad \delta m/\delta K' = 0.$$

This system is exactly solved in some limiting cases only (high and low densities). We may extend this solution to the intermediate density range since the fitting of time-resolved fluorescence traces shows a continuous variation between the two extreme ranges. Finally the impulse response I_2 for two components can be written as

$$I_2(t) = |\exp(-t/\tau_{rs}) - \exp(-t/\tau_{ds})| + \mu|\exp(-t/\tau_{rf}) - \exp(-t/\tau_{df})|,$$

where the ratio of integrated intensities of the fast and slow components F/S is given by

$$\mathrm{F/S} = \mu|(\tau_{df} - \tau_{rf})|/|(\tau_{ds} - \tau_{rs})|,$$

where $\tau_{rf} = K_{rf}^{-1}$ and $\tau_{df} = K_{df}^{-1}$ are the rise and decay times of the fast component, and $\tau_{rs} = K_{rs}^{-1}$ and $\tau_{ds} = K_{ds}^{-1}$ the rise and decay times of the slow one.

With this model five parameters have to be determined by the fitting procedure. As discussed in Ref. 2, the interpretation of these results relies on the concept of pseudoreservoir. τ_r and τ_d define the position of the pseudoreservoir in the decay sequence. This position allows us to identify these times with the sum of the characteristic times of processes acting above and below the pseudoreservoir. In the limiting cases, the position is well defined. At low density it is at the vicinity of the high vibrational levels, and the temporal characteristics of the emission are those of these states. At high density, the pseudoreservoir coincides with the relaxed state and becomes a true reservoir, with a constant decay time which is the radiative decay time of the relaxed state. The complexity of the intermediate range can be interpreted as follows: The pseudoreservoir moves steadily from intermediate levels to the lowest excited level when the density is increased. Indeed, in this density range, the evolution of decay rates is due to both the evolution with density of the position—downwards in energy—of the pseudoreservoir and that of the characteristic times. This description is quite satisfactory since it takes into account a pseudoreservoir which plays the role of an intermediate state, or of a group of intermediate vibrational levels, and allows us to assign the measured rise and decay times to the characteristic times of the decay sequence in a specific density range.[2]

The density range up to 15×10^{18} cm^{-3}, where a single component exists, provides an excellent opportunity to compare the results given by both the three- and two-exponential formalisms.

V. ANALYSIS

In the whole fitting procedure the source function has to be taken into account since the source duration is not negligible compared with the measured characteristic times. This is done by a direct convolution of the source function with the impulse responses defined above.

Figure 3 shows examples of fits of experimental curves by a (2×2) exponential model. Figure 9 presents the evolution of the involved parameters with density. As stated above, the behavior of these rates will require further interpretation apart from some clear limiting cases. In particular, at increasing pressure, the decay constant of both components tends toward an asymptotic value: This characteristic feature allows the determination of the relaxed excimer lifetimes in agreement with the model predictions. For the slow component we have determined the radiative lifetime to be $\tau_{1u} = 265$ (5) ns, while a value $\tau_{0_u^+} = 3.4$ (5) ns was obtained for the fast component. In the latter case, a better accuracy was not attainable due to the rather broad temporal width of our system. These values are in excellent agreement with the values published by Bonifield *et al.*[12] [$\tau_{1u} = 264$ (5) ns, and $\tau_{0_u^+} = 3.4$ (3) ns]. At this point, as for argon and xenon, the long component lifetime has to be interpreted as the lifetime associated with the pair of coupled states 1_u, 0_u^- in which the 0_u^- state does not decay radiative-

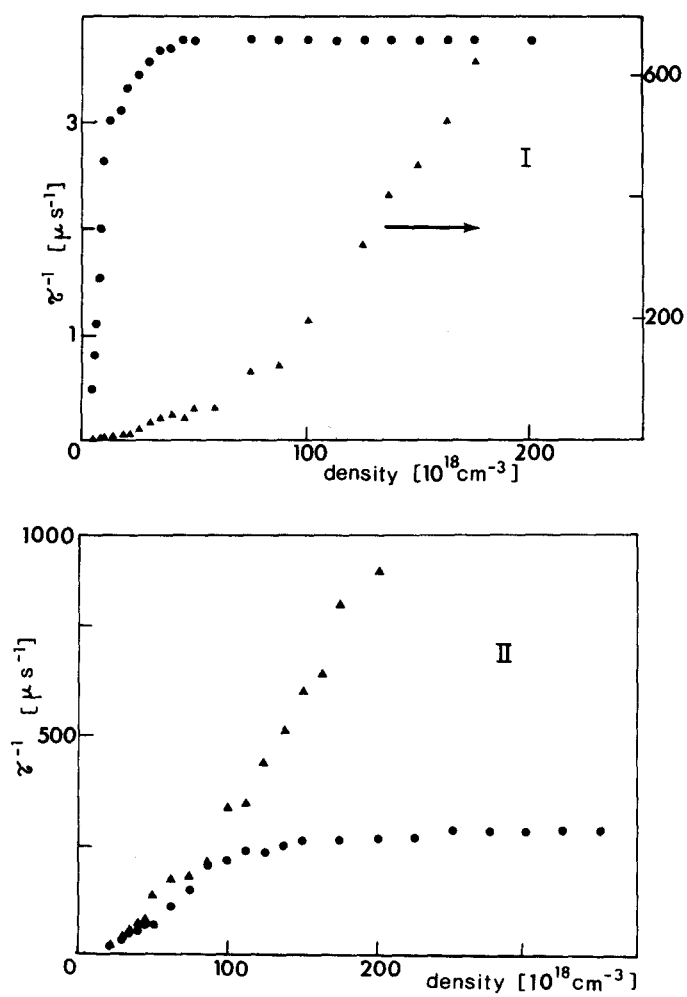

FIG. 9. Variation vs Kr density of the experimental characteristic rates [(2×2)-exponential model]. ▲: rise; ●: decay. (I) Slow component. (II) Fast component.

TABLE I. Assignment of characteristic times to physical processes, and analytic formula for the corresponding rates.

	Density range	Rise τ_r	Analytic form for τ_r^{-1}	Decay τ_d	Analytic form for τ_d^{-1}	$\tau_r+\tau_d$	Analytic form for $(\tau_r+\tau_d)^{-1}$
Fast component	Low density $d<200\times10^{18}$ cm^{-3}	τ_1	k_1d^2	$\tau_5+\tau_{0_u^+}$	$k_5d^2/(1+\tau_{0_u^+}k_5d^2)$		
	High density $d>200\times10^{18}$ cm^{-3}	$\tau_1+\tau_5$	k_fd^2	$\tau_{0_u^+}$	$\tau_{0_u^+}^{-1}$	$\tau_1+\tau_5+\tau_{0_u^+}$	$k_fd^2/(1+\tau_{0_u^+}k_fd^2)$[a]
Slow component	Low density $d<50\times10^{18}$ cm^{-3}	τ_1	k_1d^2	$\tau_2+\tau_{1u}$	$k_2d^2/(1+\tau_{1u}k_2d^2)$		
	High density $d>50\times10^{18}$ cm^{-3}	$\tau_1+\tau_2$	k_sd^2	τ_{1u}	τ_{1u}^{-1}	$\tau_1+\tau_2+\tau_{1u}$	$k_sd^2/(1+\tau_{1u}k_sd^2)$[a]

[a] $k_f=k_1k_5/(k_1+k_5), k_s=k_1k_2/(k_1+k_2)$.

ly. So, in practice, a value of $(2/3)\times265\approx178$ ns has to be considered for the relaxed 1_u state, as explained in Refs. 1 and 2.

Apart from this case where direct interpretation is possible, we have to consider separate density ranges that are not *a priori* the same for each component. An assignment of the characteristic times often remains possible according to the model introduced above, i.e., in terms of the times associated with the basic processes. Such an assignment is based on the identification of the pseudoreservoir position and is summarized in Table I. It allows us to settle the mathematical expressions to be fitted to the experimental $\tau_{r,d}$, also given in Table I. In these expressions the k_j are defined by $K_j=k_jd^2$: actually, processes (p_1) and (p_2) are expected to be quadratic (three-body collisions). As for k_5, it is introduced in Table I for the sake of clarity and results directly from a self-consistency requirement (Sec. VI).

It is clear that a single formula cannot account for the curves of Fig. 9 in the whole density range. Nevertheless, we notice that, for each component, the sum of the two characteristic times is represented by the same analytical formula in the two extreme density ranges. A monotonous change with density is exhibited for these sum values, as deduced from Fig. 9 and represented in Fig. 10. These sums appear to be nearly conservative quantities since a good accuracy is also achieved in the intermediate density range, where rather poor τ_r, and τ_d unicity is obtained. That is confirmed when comparing these sums with the three-term sums obtained by applying the three-exponential model presented now.

The previous knowledge of the radiative lifetimes allows to fix the third time of this model in the whole applicability range so that the fit is searched for with two free parameters only. It is remarkable that good fits are obtained with such a constraint. The evolution with density of the other two decay rates is presented in Fig. 11.

VI. RESULTS AND SELF-CONSISTENCY

Now, we shall see that the model and the deduced results lead in a self-consistent way to the knowledge of the rate constants.

A. k_1 and k_2 determination

As expected the variation vs density of K_1 and K_2 introduced in the three-exponential model can be fitted to a qua-

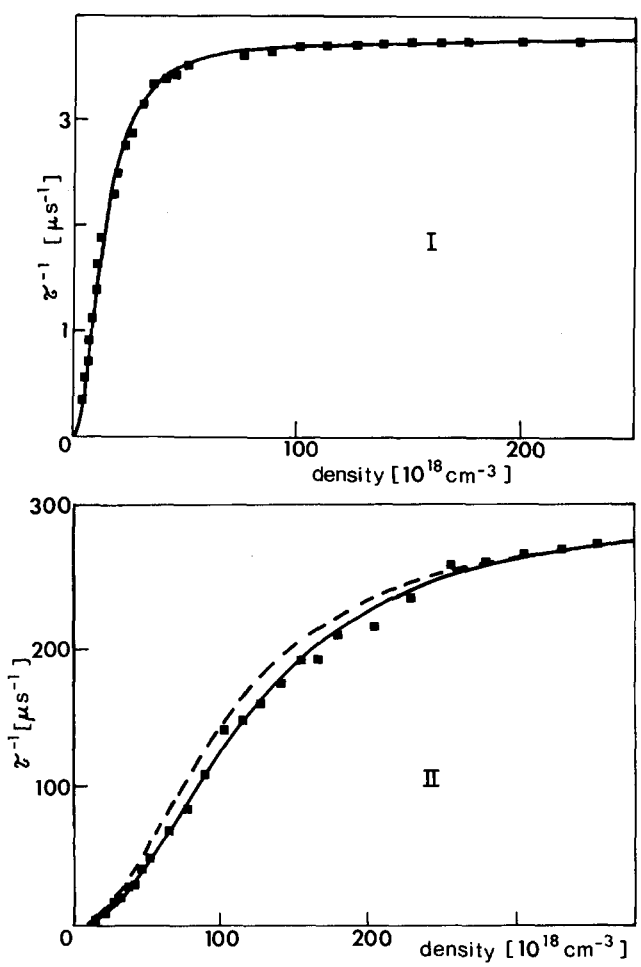

FIG. 10. Reciprocal of the time sum ($\tau^{-1}=[\tau_r+\tau_d]^{-1}$). (I) Slow component. (II) Fast component. The experimental points are deduced from Fig. 9. The curves are calculated according to the method described in Sec. VI D.

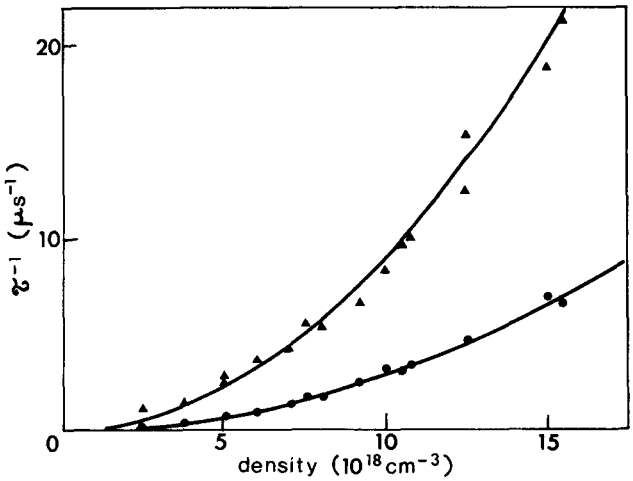

FIG. 11. Results obtained for the two decay rates τ_1^{-1}(●) and τ_2^{-1}(▲) when using the three-exponential model with a third fixed decay corresponding to $\tau_{1u} = 265$ ns. Full lines: quadratic density dependence with $\tau_1^{-1} = 2.9\times10^{-32}\,d^2$ and $\tau_2^{-1} = 9\times10^{-32}\,d^2$ (d: krypton density).

dratic law so that k_1 and k_2 values are deduced (Fig. 11). From a least-squares fit one gets

$$k_1 = 2.9\times10^{-32}\ \text{cm}^6\ \text{s}^{-1},$$
$$k_2 = 9.0\times10^{-32}\ \text{cm}^6\ \text{s}^{-1}.$$

B. Intensity ratio of fast to slow components

The variation vs density of the fast to slow components intensity ratio (F/S) is represented in Fig. 12. A quite constant value is obtained for densities above 60×10^{18} cm^{-3}. Such a characteristic feature has also been mentioned by Bonifield for krypton,[12] who evaluated this ratio to be 0.2. A constant ratio was also found in the case of xenon[2] while a slightly increasing ratio was reported for argon.[1]

According to the model, the ratio has to be interpreted as K_5/K_4 and its constancy (0.21) at high density is expected if both K's exhibit the same density dependence. Actually, this ratio reflects the competition between processes acting in the neighborhood of the crossing point (C in Fig. 4). A constant value is observed only when process (p_6) vanishes (first continuum).

Figure 13 represents the second continuum total fluorescence (fast + slow component), which indeed becomes constant at 60×10^{18} cm^{-3}. This very direct experimental result confirms what was established through the model, i.e., that the fast component does not grow above 60×10^{18} cm^{-3} and the total amount of excitation is transferred to the relaxed excimer states. In Fig. 12 the steep rise at low density is also partly due to a reduced number of primary excited atoms since a 0.7 nm excitation bandwidth is used, so that absorption is not complete.[3]

It was stated previously that the fast component appears at about 15×10^{18} cm^{-3}. In the density range (15–$60)\times10^{18}$ cm^{-3} it is not possible to reach accurate results for several reasons: (i) the process (p_6) is still acting; (ii) the fast component is growing; (iii) both components are rather imbricated since the characteristic times involved in the 2×2-exponential fits are not very different.

C. k_4 and k_5 determination

In the case of the fast component the (2×2)-exponential model takes into account, in principle, the vibrational relaxation (p_5). In practice, the related kinetic constant could be determined only if the relaxation time is not too short compared to the dimer formation time. One might expect a dependence for K_5: $K_5 = k_5\,d^2 + k'_5\,d$. At low density the limited accuracy and the competition with (p_6) do not allow to determine safely a k'_5 value. As for the density range above 60×10^{18} cm^{-3}, full self-consistency between all the involved rates is only achieved when introducing a quadratic density law for K_5, which is expected at high density. So, in practice, we shall only consider $K_5 = k_5\,d^2$, with an estimated value 10^{-31} cm^6 s^{-1} for k_5 (as detailed in Sec. VI D). As a consequence of the K_5/K_4 constancy a quadratic K_4 depen-

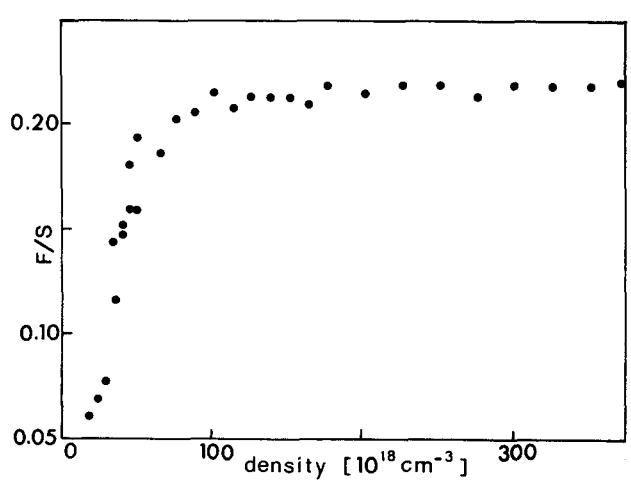

FIG. 12. Variation vs Kr density of the ratio F/S of the integrated intensities of fast and slow components.

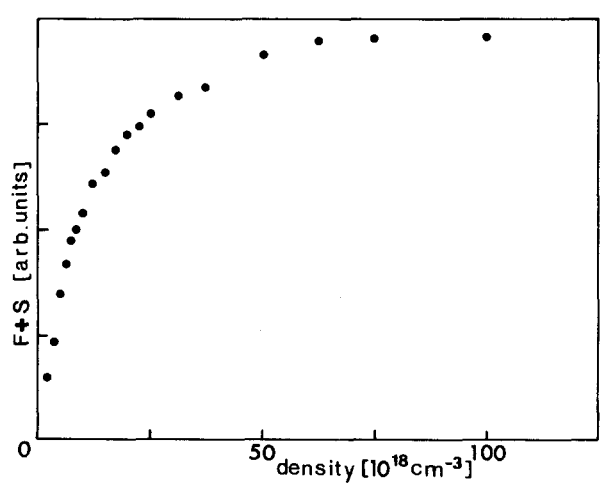

FIG. 13. Variation vs Kr density of the sum F + S of the integrated intensities of fast and slow components.

dence also has to be considered and one introduces a coefficient k_4 such as

$$K_4 = k_4 d^2 \quad \text{with } k_4 \approx 5\times 10^{-31}\ \text{cm}^6\ \text{s}^{-1}.$$

D. Self-consistency

The interpretation of the results and of the curves of Fig. 9 is closely related to the concept of pseudoreservoir stated in Sec. IV B. To each couple (τ_r,τ_d) corresponds a position of the pseudoreservoir. At a fixed density the uncertainty of that position leads to a reduced accuracy in determining τ_r and τ_d. Only their sum remains well defined. For the slow component, the sum depends on τ_1 and τ_2, which have been determined at low density, and on τ_{1u} determined at high density. So all the parameters of the mathematical function in Table I are known. That function is plotted in Fig. 10(I). A remarkably good agreement with the experimental points is obtained.

A similar treatment is possible for the fast component. In Fig. 10(II) the full line represents the corresponding formula of Table I. The dashed line is obtained by neglecting the vibrational relaxation ($\tau_5 = 0$, $k_5 = \infty$). As the other parameters are fixed, we see that τ_5 has to be introduced for the coherence of results.

Now, we can explain the evolution of each characteristic time (Fig. 9) especially in the density ranges $(5\text{–}15)\times 10^{18}\ \text{cm}^{-3}$ for the slow component, and $(50\text{–}150)\times 10^{18}\ \text{cm}^{-3}$ for the fast one, ranges in which the respective τ_r and τ_d are almost equal. Owing to the absolute values in the (2×2)-exponential formula no sign change can be evidenced. It is realistic to decide that the shorter time in the fit is the rise time while the longer one is the decay time. We have then to wonder if a crossing in the interpreted times occurs.

For the slow component in the low density range $(5\text{–}15)\times 10^{18}\ \text{cm}^{-3}$ one has: $\tau_{rs}\approx\tau_1, \tau_{ds}\approx\tau_2+\tau_{1u}$ with $\tau_1 = (k_1 d^2)^{-1}, \tau_2 = (k_2 d^2)^{-1}$ (Table I). Then, we can determine the density at which $\tau_1(d) = \tau_2(d) + \tau_{1u}$. One finds $d = 9.4\times 10^{18}\ \text{cm}^{-3}$. Such a result allows us to conclude that at this density, $\tau_{rs} = \tau_{ds} = \tau_1 = \tau_2 + \tau_{1u}$. Furthermore, since this density corresponds to a crossing of the rates additional interpretation can be given. Below $9\times 10^{18}\ \text{cm}^{-3}$ the longer time is no more monitored by $\tau_2 + \tau_{1u}$ but by τ_1, and the shorter by $\tau_2 + \tau_{1u}$. Actually, if we draw the curves τ_1^{-1} and $(\tau_2 + \tau_{1u})^{-1}$ according to this interpretation and the formula given in Table I for the low density range, a very nice agreement with the above conclusion is obtained [Fig. 14(I)].

Finally it must be emphasized that the observed crossing in the two-exponential model is inherent to the crudeness of the mathematical model since, in the more sophisticated three-exponential one, each characteristic time is correlated to a single physical process.

In this interpretation of the slow component the results given by the three-exponential model for the sum of characteristic times are consistent with those given by the (2×2)-exponential model. The interpretation implies that, at low density, the pseudoreservoir is situated at the $^3P_2$ atomic state on both sides of the rate crossing point in Fig. 14(I). It

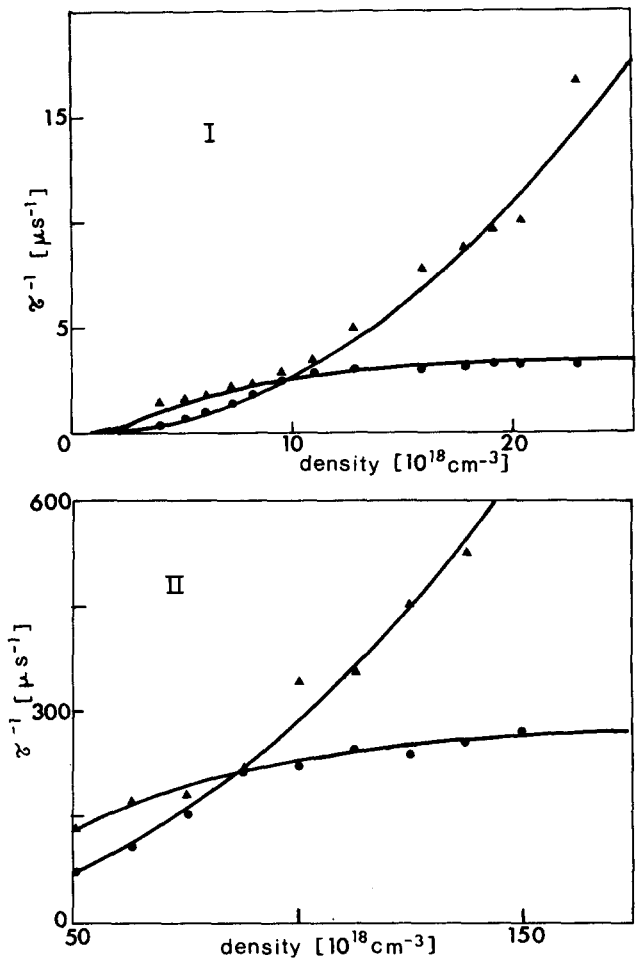

FIG. 14. Result of the interpretation of the rate crossing (see the text). Experimental data correspond to part of those given in Fig. 9, plotted at an expanded scale. (I) Slow component. (II) Fast component.

implies also that $\tau_1 > \tau_2$ which was already established for xenon.[2] Such a result is satisfactory for basic reasons. Indeed, while the $1_u,0_u^-$ state is triply degenerate and 0_u^+ is not, a higher $1_u,0_u^-$ dimer formation probability is expected since more favorable configurations are involved. Futhermore, the interpretation of the results obtained at high density, in particular from the fast component behavior, will provide other arguments to self-consistency.

From inspection of Fig. 9(II) it seems that there is also a rate crossing for the fast component at high density. The same analysis as before still holds, so that one may conclude that: (i) there is a crossing at $85\times 10^{18}\ \text{cm}^{-3}$ in the two-exponential description of the fast component; (ii) at this crossing $\tau_{rf} = \tau_{df} = \tau_1 = \tau_5 + \tau_{0_u^+}$.

As was done for the slow component, it is possible, with the help of this interpretation, to describe the evolution of τ_{rf} and τ_{df} separately, as shown in Fig. 14(II) and according to the formula given in Table I. It is remarkable that the value of k_1 used in this high density fast component description is the same as that used at low pressure for the slow component. It is a new argument for self-consistency and a striking confirmation of our previous conclusion, i.e., $\tau_1 > \tau_2$. It has

to be noticed that the curves given in Fig. 14(II) are calculated using again $k_5 = 10^{-31}$ cm^6 s^{-1} in the density range where the τ_5 values are the most significant.

The interpretation now being well settled, we can look further into the pseudoreservoir concept. Actually our interpretation is closely related to the knowledge of its energy position at each density, as we now discuss. If we consider the rise time of the slow component as compared to the τ_1 and $\tau_1 + \tau_2$ curves (Fig. 15) it indicates clearly that above 50×10^{18} cm^{-3} that rise time is no more monitored by τ_1 but by $\tau_1 + \tau_2$. The transition from one description to the other takes place when density approaches 50×10^{18} cm^{-3}, thus indicating that the pseudoreservoir moves from $^3P_2$ to $1_u, 0_u^- v = 0$ in the neighborhood of this density. This change occurs in a limited density range without any dramatic apparent effect since $\tau_2 < \tau_1$. This density explicitly determines the frontier between what we call low and high densities for the slow component in Table I. These results are illustrated in Fig. 16(I) where the two regimes are represented by A_s (reservoir around the $^3P_2$ atomic level), and B_s (reservoir at $1_u v \approx 0$ level).

As for the fast component, one may conclude similarly that at densities near the rate crossing the pseudoreservoir is near C point of Fig. 4 ($0_u^+, v \gg 0$). When the pressure increases τ_5 decreases, and τ_{df} tends towards $\tau_{0_u^+}$, so that above 200×10^{18} cm^{-3} the decay is practically monitored by $\tau_{0_u^+}$ and the pseudoreservoir can be considered as coinciding with the relaxed ($0_u^+, v \approx 0$) excimer level. The two regimes are represented by A_f and B_f in Fig. 16(II). For completion, in Fig. 16(I), we introduce at very low density (below that of our experiments) the regime $\tau_r \approx \tau_2$ and $\tau_d \approx \tau_1$, since $\tau_1 > \tau_2 \gg \tau_{1u}$ in this case.

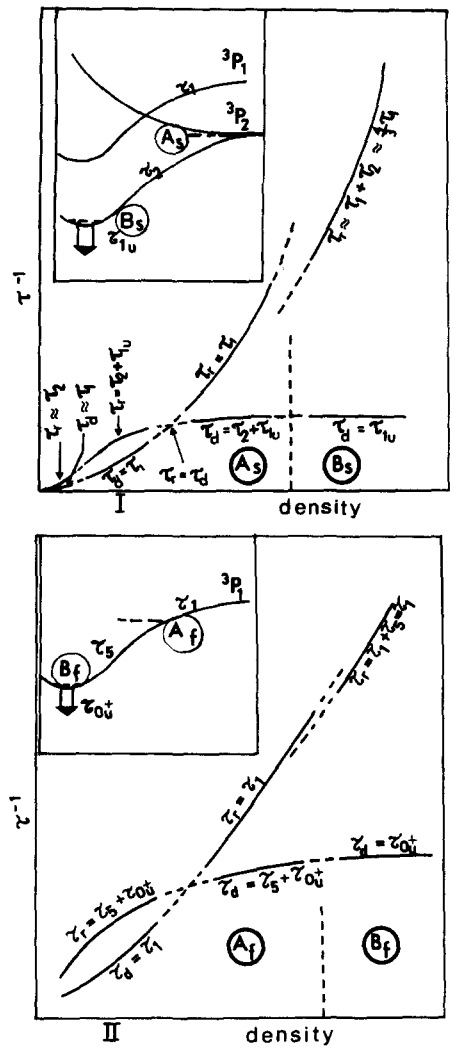

FIG. 16. Summing up of the interpretation of rise and decay rates [(2×2)-exponential model] in terms of the basic process rates, relying on the pseudoreservoir energy position shown in inset in close connection to Table I.

VII. $^1P_1$ EXCITATION: PRELIMINARY RESULTS

In several works dealing with krypton, a bottle-neck effect on the kinetics correlated to atomic states higher than $^3P_1$ has been reported but never well interpreted.[12,14] In particular, this effect is evidenced when comparing studies concerning krypton and xenon, since in xenon such an effect does not exist, as shown in Ref. 2. For example, in the study of Bonifield *et al.*[12] where both selective photoexcitation and electron beam excitation were used, the excitation of the $^1P_1$ atomic state produced decay rates whose pressure dependence was reminiscent of the results obtained from electron beam excitation.

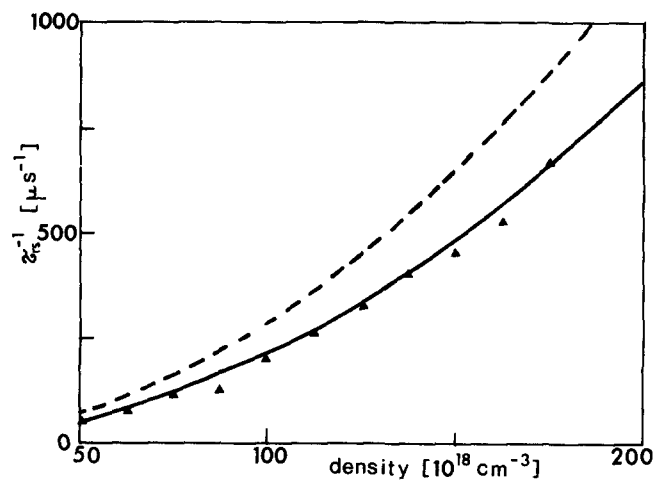

FIG. 15. Slow component rise rate τ_{rs}^{-1} in the high density range. ▲: experimental. Dashed line: $\tau^{-1} = 2.9\times10^{-32}\, d^2$. Full line: $\tau^{-1} = 2.2\times10^{-32}\, d^2$ curve associated with $\tau_1 + \tau_2$.

We have obtained some preliminary results concerning the excitation of the $^1P_1$ atomic state. Figure 17 shows, at two densities, time-resolved fluorescence curves after $^3P_1$ and $^1P_1$ excitation. It is clear that, at low density [Fig. 17(I)], the decay after $^1P_1$ excitation involves times longer than after $^3P_1$ excitation. This effect is still noticeable at high density [Fig. 17(II)]. For argon, similar observation has been tentatively explained by decay processes through the $^3P_0$ atomic level.[1]

Red or blue wing $^1P_1$ excitation gives no noticeable difference. So, as for argon, we may tentatively conclude that feeding $^3P_0$ and/or its correlated molecular states is fast but that their decay is long. Nevertheless, direct characteriza-

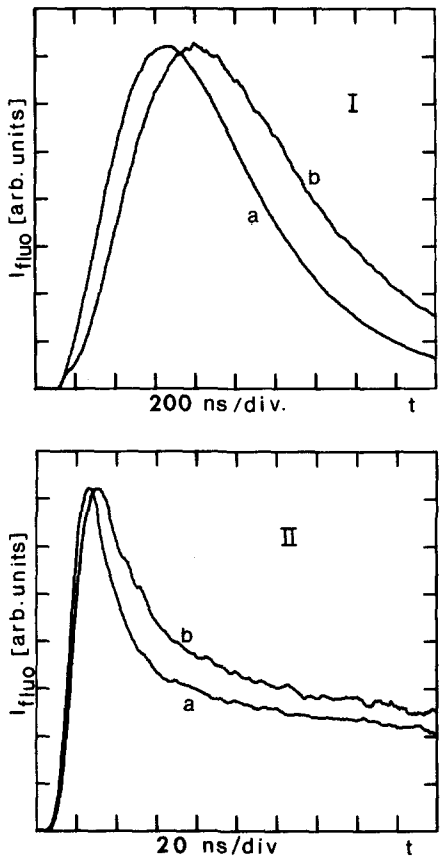

FIG. 17. Time-resolved fluorescence after $^3P_1$ (a), and $^1P_1$ (b) excitation at low [(I) $d = 10\times10^{18}$ cm^{-3}], and high [(II) $d = 300\times10^{18}$ cm^{-3}] densities.

tion of such an intermediate decay step is possible using reexcitation techniques as already demonstrated with another experimental setup.[2] These somewhat preliminary results indicate the need for both more detailed experimental data and a specific model. Such a work is now in progress.

VIII. FINAL DISCUSSION: COMPARISON WITH AVAILABLE RESULTS

Comparison of our results with those of the literature must be done with caution. Actually, available data are strongly dependent on both the experimental approach and the data analysis. Two groups of experiments have to be distinguished: (i) experiments based on selective excitation[4,9,12,15]; and (ii) experiments based on nonselective excitation.[14,16–20] In the second case, the experimental data differ considerably from ours. In principle, a suited model could provide kinetic parameters allowing comparison in some cases. Nevertheless, the comparison between our results about $^3P_1$ and $^1P_1$ excitation indicates that modeling the $^1P_1$ kinetics without the preliminary knowledge of the $^3P_1$ one is rather problematic since many unknown parameters have to be determined precluding unicity and accuracy. In particular, Janssens *et al.*,[16] who use nonselective excitation and do not separate the first and the second continua, invoke processes that we do not retain (see Sec. III B) and, per contra, do not consider as a main process the population of the $^3P_2$ level through $0_u^+, v\gg0$ excimer formation (p_1). This process was first clearly evidenced by Bonifield,[12] the only author, who until now, reported high density results. Working at high density is a prerequisite to get a well separated fast component, and subsequently a clear evidence of process (p_1) independently of process (p_2). The analysis method, although somewhat different from ours, may nevertheless be considered as an approximation of it. Indeed the fast component is not isolated by a two-component fit, as we do, but by considering a short time scale that is realistic at high density. The k_1 value then obtained is 3.2×10^{-32} cm^6 s^{-1}, which is in good agreement with our result (2.9×10^{-32} cm^6 s^{-1}). As stated above, this value allows us to also describe the low density slow component. It has to be noted that an erroneous k_2 determination is possible when using only experimental results limited up to 30×10^{18} cm^{-3}. Indeed, in numerous work on rare gases, the rise time of the slow component is assigned to 1_u excimer formation from the $^3P_2$ level (τ_2,k_2) whereas we demonstrated that $^3P_2$ feeding through $0_u^+, v\gg0$ excimer formation is a slower process. We have pointed out that in the density range where the fast component increases $(15–60)\times10^{18}$ cm^{-3}, the accuracy is reduced so that comparison with works dealing with a limited density range is somewhat dubious. Nevertheless, comparison can be attempted: in the density range $(10–60)\times10^{18}$ cm^{-3} (above the rate crossing) the slow component rise time is monitored

TABLE II. Comparison between literature data for the krypton relaxed excimer lifetimes (0_u^+, and 1_u,0_u^-, $v\approx0$ level) and the decay rates k_1 and k_2.

Authors and references	Excitation method	Density range (10^{18} cm^{-3})	k_1 (10^{-32} cm^6 s^{-1})	k (10^{-32} cm^6 s^{-1})	k_2 (10^{-32} cm^6 s^{-1})	$\tau_{0_u^+}$ (ns)	τ_{1u} (ns)
Bouciqué (Ref. 17)	*n*	1–20		4.4			1700
Leichner (Ref. 18)	*n*	1–30		0.83,2.1			295
Brodmann (Ref. 4)	*s*	1–20	2.2				
Salamero (Ref. 19)	*n*	3–30		1.8			250
Wenck (Ref. 15)	*s*	3–30	1		1.78	5.2	149
Boniefield (Ref. 12)	*s*	3–250	3.2			3.4	264
Haaks (Ref. 9)	*s*	3–30	4.0		2.6	5.2	265
Wieme (Ref. 20)	*n*	0.1–3			3.91		
Janssens (Ref. 16)	*n*	3–30	0.23		1.4		256
Firestone (Ref. 14)	*n*	3–30		1			395
This work	*s*	3–375	2.9		9.0	3.4	265

[a] *s* is for selective excitation; *n* is for nonselective excitation.

by τ_1 but was identified to τ_2 in several works for the above-mentioned reasons, i.e., in the same way as at low density. In particular, Haaks,[9] using selective excitation, obtains $k_2 = 2.6\times10^{-32}$ cm^6 s^{-1}, in very good agreement with our value: $k_1 = 2.9\times10^{-32}$ cm^6 s^{-1}, whereas we get $k_2 = 9.0\times10^{-32}$ cm^6 s^{-1}. Comparison with works using a different experimental approach is not so clear since the long times involved in the high-lying excited state decay must be taken into account. Furthermore, several authors introduce in the rates a linearly density-dependent contribution that we did not evidence.

Finally, in Table II we list values of lifetimes and rates available from the literature. The rates k_1 and k_2 are quoted when the processes are clearly identified, even if the model used invokes other processes than ours, and if reinterpretation is necessary. We introduce also somewhat unassigned k values. That corresponds to results obtained from nonselective excitation in which identification in terms of our processes is not possible, mainly due to the long-lived reservoir situated above the $^3P_1$ level. Nevertheless, in the work of Salamero *et al.*,[19] if we ascribe their smaller rate to that reservoir effect, the other value ($k = 1.8\times10^{-32}$ cm^6 s^{-1}) can be considered as comparable with the relaxed 1_u formation rate from $^3P_1$ that we define in our work from $(kd^2)^{-1} = \tau_1 + \tau_2 + \tau_4 \approx \tau_1 + \tau_2 = (k_1 d^2)^{-1} + (k_2 d^2)^{-1}$, so that $k \approx 2.2\times10^{-32}$ cm^6 s^{-1}.

IX. CONCLUSION

Combining time-resolved fluorescence, pressure effect, and selective excitation of the first resonance line of krypton around 123.6 nm we have obtained detailed information on kinetics.

All basic processes leading to the rise of a fast component in the second continuum fluorescence around 145 nm have been clearly established and the associated parameters determined. Such a progress in this subject has been possible by using, in a self-consistent way, mathematical models which have not been introduced arbitrarily but which rely on argued simplifications. We believe that a detailed knowledge of the kinetics is only attainable by combining such a method and a selective excitation. Actually the present preliminary results indicate that the $^1P_1$ decay has a very specific and nontrivial behavior as compared to the $^3P_1$ one. Therefore, nonselective excitation experiments largely deal with that effect, which explains the rather scattered results reported to date in the literature. A specific study of the $^1P_1$ decay is in progress.

[1] P. Moutard, P. Laporte, J.-L. Subtil, N. Damany, and H. Damany, J. Chem. Phys. **87**, 4576 (1987).
[2] P. Moutard, P. Laporte, N. Damany, J.-L. Subtil, and H. Damany, J. Chem. Phys. **88**, 7485 (1988).
[3] F. X. Gadea, F. Spiegelmann, M.-C. Castex, and M. Morlais, J. Chem. Phys. **78**, 12 (1983).
[4] R. Brodmann and G. Zimmerer, J. Phys. B **10**, 3395 (1977).
[5] N. Damany, P. Laporte, J.-L. Subtil, and H. Damany, Phys. Rev. A **32**, 3418 (1985).
[6] P. Laporte, N. Damany, and H. Damany, Opt. Lett. **12**, 987 (1987).
[7] P. Moutard, P. Laporte, and H. Damany, Rev. Phys. Appl. (Paris) **19**, 409 (1984).
[8] H. D. Wenck, S. S. Hasnain, M. M. Nikitin, K. Sommer, G. Zimmerer, and D. Haaks, Chem. Phys. Lett. **66**, 138 (1979).
[9] D. Haaks, *Habilitationsschrift* (R. F. A. Wuppertal, 1980).
[10] T. L. Barr, D. Lee, and F. R. Gilmore, J. Quant. Spectrosc. Radiat. Transfer **15**, 625 (1975).
[11] O. Vallée, N. Tran Minh, and J. Chapelle, J. Chem. Phys. **73**, 2784 (1980).
[12] T. D. Bonifield, Ph.D. thesis, Rice University, Houston, Texas, 1979; T. D. Bonifield, F. H. K. Rambow, G. K. Walters, M. V. Mc Cusker, D. C. Lorents, and R. A. Gutcheck, Chem. Phys. Lett. **69**, 290 (1980).
[13] E. Matthias, R. A. Rosenberg, E. D. Poliakoff, M. G. White, S. T. Lee, and D. A. Shirley, Chem. Phys. Lett. **52**, 239 (1977).
[14] R. F. Firestone and W. E. Selander, J. Chem. Phys. **88**, 717 (1988).
[15] H. D. Wenck, *Interner Bericht*, DESY/Hamburg, F 41-79/10, 1979; H. D. Wenck, M.-C. Castex, D. Haaks, M. M. Nikitin, B. Jordan, and G. Zimmerer, Proceedings of the 6th International Conference on VUV Radiation Physics, Charlottesville, 1980.
[16] H. Janssens, M. Vanmarcke, E. Desoppere, J. Lenaerts, R. Bouciqué, and W. Wieme, J. Chem. Phys. **86**, 4925 (1987); H. Janssens, M. Vanmarcke, E. Desoppere, R. Bouciqué, and W. Wieme, *ibid.* **86**, 4935 (1987).
[17] R. Bouciqué and P. Mortier, J. Phys. D **3**, 1905 (1970).
[18] P. K. Leichner and R. J. Ericson, Phys. Rev. A **9**, 251 (1974).
[19] Y. Salamero, A. Birot, M. Brunet, J. Galy, P. Millet, and J. P. Montagne, J. Phys. B **12**, 419 (1979).
[20] W. Wieme and J. Lenaerts, J. Chem. Phys. **74**, 483 (1981).